*Molecular Physics*, 2015
Vol. 113, Nos. 15–16, 2063–2072, http://dx.doi.org/10.1080/00268976.2014.921342





## INVITED ARTICLE

# The $^2\Pi$–$\widetilde{X}^2\Pi$ electronic spectra of long carbon-chain $^{(13)}C_{2n}H/D$ molecules for ($n = 4$–6)

M.A. Haddad[a,*], D. Zhao[b], H. Linnartz[a,b] and W. Ubachs[a]

[a]*Department of Physics and Astronomy, LaserLaB, VU University, Amsterdam, The Netherlands;* [b]*Sackler Laboratory for Astrophysics, Leiden Observatory, University of Leiden, Leiden, The Netherlands*

(*Received 20 February 2014; accepted 1 May 2014*)

Unresolved $^2\Pi$–$\widetilde{X}^2\Pi$ electronic origin band transitions have been measured for the even-numbered linear carbon-chain radicals $^{(13)}C_{2n}H/D$ with $n = 4$–6. Spectra of the fully $^{13}C$ substituted $^{13}C_8H/D$ and $^{13}C_{10}H/D$ isotopologues are presented for the first time. $^{12}C_{10}H/D$ and $^{12}C_{12}H/D$ spectra are presented with improved signal-to-noise ratio to realise a systematic study of the band profiles. Despite the fact that individual rotational transitions cannot be resolved, it is possible to derive effective values for the upper state lifetime. The obtained natural lifetime line broadening parameters of $0.8 \pm 0.1$ cm$^{-1}$ for $n = 4$, $4.0 \pm 0.5$ cm$^{-1}$ for $n = 5$ and $4.8 \pm 0.5$ cm$^{-1}$ for $n = 6$ indicate that internal conversion processes occur in these carbon-chain molecules.

**Keywords:** cavity ring-down spectroscopy; electronic spectroscopy; carbon-chain radicals; $C_{12}H$; $C_{12}D$; $^{13}C_8H$; $^{13}C_{10}H$

## 1. Introduction

Highly unsaturated hydrocarbons of the form $C_nH$ have proven important intermediates in the chemistry of the interstellar medium. Their large dipole moment makes them ideally suited to search for in dark clouds by radio astronomy and positive identifications have been reported for $C_3H$ [1], $C_4H$ [2], $C_5H$ [3], $C_6H$ [4], $C_7H$ [5] and $C_8H$ [6–8]. Also, the chemically related anionic species, $C_4H^-$ [9], $C_6H^-$ [10] and $C_8H^-$ [7,11] have been detected in space. In the laboratory, spectra of substantially longer chains have been studied. Using Fourier-transform microwave spectroscopy, accurate rotational ground-state constants have been derived for chains as long as $C_{14}H$ [12–14]. Also in the optical domain strong electronic spectra of even $C_{2n}H$ and odd $C_{2n+1}H$ chains have been reported, using a variety of different spectroscopic techniques, both matrix based [15] and in the gas phase, such as cavity ring-down spectroscopy (CRDS), resonance enhanced multiphoton ionization time of flight (REMPI-TOF) and incoherent broad band cavity enhanced spectroscopy (IBBCEAS) [16,17]. A fully resolved rotational spectrum has been reported for the two spin–orbit components of the $^2\Pi$–$\widetilde{X}^2\Pi$ electronic origin band system of $C_6H$ and $C_6D$ [18] that was reinterpreted recently in terms of an extensive Renner–Teller analysis [19]. In contrast, no rotationally resolved spectra have been recorded for the $^2\Pi$–$\widetilde{X}^2\Pi$ electronic origin band transition of $C_8H$ ($C_8D$) and $C_{10}H$ ($C_{10}D$) [20]. Even in a continuous wave-CRDS experiment [21] with a laser bandwidth far below the expected rotational spacing between adjacent $C_8H$ rotational lines, only unresolved P- and R-branch envelopes were found and a lifetime of ~7 ps was derived for the $^2\Pi_{3/2}$ upper electronic state to explain this observation. Also, in contrast to $C_6H$, only the contour of one P- and R-branch system could be observed for $C_8H$. This is likely because of spectral overlap of the $\Pi_{3/2}$–$\widetilde{X}^2\Pi_{3/2}$ and $\Pi_{1/2}$–$\widetilde{X}^2\Pi_{1/2}$ spin–orbit bands (i.e. $|A'' - A'| \sim 0$) in combination with a low population density in the $\widetilde{X}^2\Pi_{1/2}$ upper spin–orbit state. For $C_{10}H$ ($C_{10}D$) and $C_{12}H$ ($C_{12}D$) even, no separate P- and R-branches were found. Instead, the bands reported so far [22,23] exhibit rather broad and largely unstructured profiles.

This study extends and complements previous work on the longer $C_{2n}H$ radicals, largely investigated some 15 years ago. The spectra have a somewhat better signal-to-noise ratio (S/N) and in combination with other spectroscopic constants that have become available meanwhile, this now allows to systematically investigate lifetime broadening effects. Moreover, a higher sensitivity combined with isotopically enriched gas samples makes it possible to also record spectra of isotopes previously not accessible, specifically $^{13}C_8H$, $^{13}C_8D$, $^{13}C_{10}H$ and $^{13}C_{10}D$ for which the first $^2\Pi$–$\widetilde{X}^2\Pi$ spectra are presented here. Assignments to these bands are possible because of the involved isotopic shifts.

## 2. Experimental

Pulsed CRDS is used to record direct absorption spectra of the $C_{2n}H$ chains through a supersonically expanding hydrocarbon plasma. High pressure mixtures (~10 bar) of 0.5%$^{12}C_2H_2$, 0.2%$^{12}C_2D_2$ and 0.2%$^{13}C_2H_2$ diluted in

* Corresponding author. Email: m.a.haddad@vu.nl

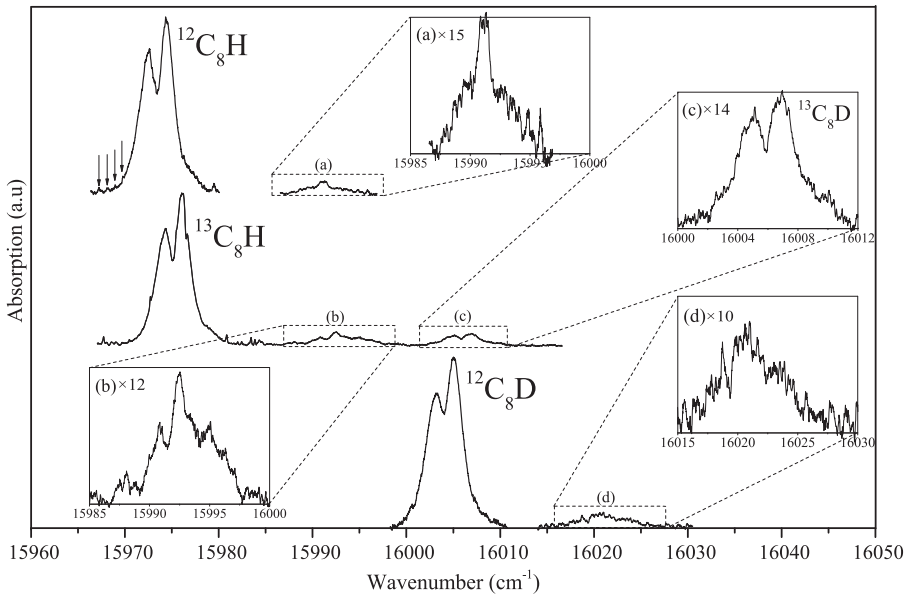


Figure 1. The $^2\Pi$–$\widetilde{X}^2\Pi$ electronic origin band transition of $C_8H$ (upper trace), $^{13}C_8H$ (middle trace) and $C_8D$ (lower trace) observed by cavity ring down spectroscopy in a pulsed pinhole jet plasma. The weak origin band of the $^2\Pi$–$\widetilde{X}^2\Pi$ electronic transition of $^{13}C_8D$ is shown in panel (c) and an unstructured component of a sequence transition of the lowest frequency bending mode (see Ref. [20]) is shown in panels (a), (b) and (d) for $C_8H$, $^{13}C_8H$ and $C_8D$, respectively. The arrows at the left side of the $^{12}C_8H$ spectrum indicate weak but sharp observed features of *l*-$C_3H_2$.

He/Ar ∼ 1:1 gas are discharged in the throat of a modified pinhole nozzle [24,25] to generate $^{(12/13)}C_{2n}H/C_{2n}D$ radicals in a circular expansion. A regular vacuum (0.05 mbar during plasma operation) is maintained by a roots blower pump (1000 m$^3$ h$^{-1}$). A negative high-voltage pulse ∼300 $\mu$s is applied to the (500 $\mu$s long) expanding gas pulse, typically with $V/I \approx -1$ kV/100 mA. The distance of the pinhole nozzle orifice to the optical cavity axis can be varied during jet operation between 0 and 30 mm which allows to record spectra at different rotational temperatures.

Tunable light at around ∼625, ∼714 and ∼800 nm is generated by a pulsed dye laser (Sirah, Cobra Stretch) with Rhodamine 101, Pyridine 2 and Styryl 11, respectively, pumped by a frequency-doubled Nd:YAG laser (532 nm). The pulsed dye laser system is operated at an 8 Hz repetition rate with a pulse width of ∼6 ns and a bandwidth narrower than 0.05 cm$^{-1}$. The best achievable resolution – also taking into account residual Doppler broadening in the pinhole expansion – yields an upper limit ∼0.12 cm$^{-1}$, i.e., far more than a typical 2*B* value for the chains studied here.

A cavity ring-down event is initiated by injecting laser light into a high-finesse optical cavity, consisting of two highly reflective plano-concave mirrors, positioned 58 cm apart, that are mounted on high precision alignment tools and located on opposite sides of a high vacuum chamber. The light leaking out of the cavity is detected by a photomultiplier tube to record the ring-down decays. Non-linear scanning of the laser frequency is corrected by simultaneously recording the transmission fringes of two solid etalons (with free spectral ranges (FSR) ∼20.1 and 7.57 GHz). In the case of $^{(12/13)}C_8H/D$ (around 625 nm), an absolute laser frequency calibration is achieved by simultaneously recording an iodine reference spectrum with a precision better than 0.02 cm$^{-1}$. The $C_{10}H$ and $C_{12}H$ chains absorb around 714 and 800 nm, where iodine only weakly absorbs. Here, an absolute calibration is derived from resolved ro-vibrational $C_2$ transitions that are recorded simultaneously and that originate from the Philips and Swan band systems [26,27].

## 3. Results

### 3.1. $C_8H$, $C_8D$, $^{13}C_8H$ and $^{13}C_8D$

In Figure 1 overview, spectra are shown for the $^2\Pi$–$\widetilde{X}^2\Pi$ electronic transitions of $C_8H$ (upper trace), $^{13}C_8H$ (middle trace) and $C_8D$ (lower trace). The spectra comprise of unresolved P- and R-branches, originating from the $\Pi_{3/2}$–$\widetilde{X}^2\Pi_{3/2}$ and the $\Pi_{1/2}$–$\widetilde{X}^2\Pi_{1/2}$ spin–orbit transitions. The $C_8H$ and $C_8D$ spectra are found at very similar positions as reported in Ref. [20], i.e., overlapping within experimental uncertainties. Also other previously observed features, such as a weak component a few cm$^{-1}$ towards higher energy, are reproduced. This is shown in detail in the insets (a), (b) and (d) in Figure 1.

The $^{13}C_8H$ band, which has not been reported before, is located at 15,975.1 cm$^{-1}$, ∼2 cm$^{-1}$ blueshifted with respect to the band found for $C_8H$. The $^{13}C_8H$ spectrum shows several similarities with the $C_8H$ and $C_8D$ spectra. A weaker

feature near ∼15,993 $cm^{-1}$ (Figure 1(b)) is the equivalent of the bands shown in (a) and (d); this absorption peak has a similar shift with respect to the main spectrum as found for these two bands. However, the band at ∼16, 006 $cm^{-1}$, shown in Figure 1(c) has no direct equivalent in the $^{12}C$ spectra. Figure 1(c) shows that this feature has a profile that is very similar to the origin band spectra of $C_8H$, $C_8D$ and $^{13}C_8H$. The spectrum is ∼2 $cm^{-1}$ blueshifted with respect to $C_8D$, i.e., similar to the value found for $C_8H$ and $^{13}C_8H$. Therefore, its appearance is fully consistent with an assignment to $^{13}C_8D$, although this is not a priori expected from the used precursor species. As a $^{13}C_2H_2$/He/Ar mixture is used, an assignment to $^{13}C_8D$ only can be explained with a remaining pollution in the gas bottle with deuterated acetylene used in an earlier experiment or by a D-enrichment in the $^{13}C_2H_2$ precursor gas. This has been checked by Fourier-transform infrared spectroscopy of the used precursor gas sample, confirming that the sample indeed contains a few per cent (i.e. more than natural abundance) of $^{12}C_2D_2$. This may in principle cause the production of trace amounts of $^{12}C/^{13}C$ mixed isotopologues of carbon-chain species. However, in previous experiments using the same gas mixture to record $^{13}C_3$ no clear signals for $^{12}C^{13}C_2$ were found [28]. From this, we conclude that the $^{12}C$ abundance in the $^{13}C$-enriched sample is only present in a minute quantity and in worst case would have a negligible effect on the overall spectroscopic features.

The origin of the weaker bands positioned at ∼15,991 $cm^{-1}$(for $C_8H$) and ∼16,020 $cm^{-1}$ (for $C_8D$) has been discussed in Ref. [20]. Now, also a similar spectral feature (see Figure 1(b)) is found at ∼15,993 $cm^{-1}$ for $^{13}C_8H$ obtained with a $^{13}C$-enriched precursor gas. As stated before, it is likely that the strong band system around 15,975.1 $cm^{-1}$ comprises both the $^2\Pi_{3/2}$–$\widetilde{X}^2\Pi_{3/2}$ and $^2\Pi_{1/2}$–$\widetilde{X}^2\Pi_{1/2}$ bands, with the latter one much less populated for the low temperatures in the jet expansion. This leaves the weaker bands, ∼17 $cm^{-1}$ blue shifted with respect to the maxima in the spectra of all three isotopologues, as to originate from a low-lying vibrationally excited species, consistent with the findings discussed in Ref. [20].

Several spectra have been recorded by changing the distance between nozzle orifice and optical axis of the cavity. This allows to vary the rotational temperature in a range from ∼5 to ∼40 K. The resulting spectra are analysed by contour fitting using a standard Hamiltonian for a $^2\Pi$–$\widetilde{X}^2\Pi$ transition by PGopher software [29]. Separate fits are performed for $C_8H$, $C_8D$ and $^{13}C_8H$ to derive the optimum values of parameters and minimal fit residuals. The ground-state parameters $B''$ and $A''$ of $C_8H$ are fixed to available microwave data [12,14] and the excited-state constant $B'$, band origin $T_{00}$ as well as Lorentzian line width Γ and temperature $T_{rot}$ are varied to reproduce the spectral profiles.

In the case of $C_8D$ and $^{13}C_8H$, for which accurate ground-state parameters are not available from microwave data, the value of $A''$ is kept the same as for $C_8H$, while the rotational constants are fixed to values derived from density functional theory (DFT) calculations at the B3LYP/3-21G* level. These DFT calculations are performed using the Gaussian 03 software package [30], yielding values of $B''_e = 0.019617$ $cm^{-1}$ (for $C_8H$), $B''_e = 0.018961$ $cm^{-1}$ (for $C_8D$) and $B''_e = 0.018153$ $cm^{-1}$ (for $^{13}C_8H$). The calculated value of $B''_e$ for $C_8H$ deviates less than 1% from the measured value of $B''_0 = 0.019589$ $cm^{-1}$ in Ref. [12,14]. In view of these accurate predictions and because it is not possible to constrain both ground- and excited-state rotational constants from the unresolved spectra, the $B''_0$ values for $C_8D$ and $^{13}C_8H$ are fixed to the $B''_e$ values. With this assumption, it is possible to extract the upper state parameters $B'$ and $T_{00}$ as well as Lorentzian line widths Γ from a fitting routine. It is found from different fits that variations within ±1% in the values of the fixed ground-state constants do not significantly change the final fitting results. In all fits, special care has been taken to check the correlation factor between the floating parameters, to guarantee that the derived parameters reflect unique and uncorrelated values. Further details of these fits are discussed below. In addition, considering that the experimental spectra may be affected by plasma instabilities and the trace absorption of other isotopologues, the resulting parameters of the individual fits are taken with three times standard deviation.

It is known that the $^2\Pi_{1/2}$–$\widetilde{X}^2\Pi_{1/2}$ transition is hidden under the strong $^2\Pi_{3/2}$–$\widetilde{X}^2\Pi_{3/2}$ transition [20], which is much stronger – for low temperatures – in all even-numbered $C_{2n}H$ chains studied here, as these exhibit an inverted spin–orbit structure, i.e., with $\widetilde{X}^2\Pi_{3/2}$ as the lower level. In view of the rather large value of the spin–orbit splitting $A'' = -19.34$ $cm^{-1}$ for $C_8H$, the $^2\Pi_{1/2}$–$\widetilde{X}^2\Pi_{1/2}$ component starts to contribute a significant intensity to the spectrum only for internal temperatures of $T_{rot} \gtrsim 30$ K (assuming thermal equilibrium between spin–orbit and rotational excitations). For the lower $T_{rot}$ values, therefore, mainly the lower spin–orbit component contributes to the spectral appearance.

Several spectra were recorded in the pinhole plasma expansion for ∼15 mm downstream at ∼7–9 K, displayed in Figure 2(a), 2(c) and 2(e) for which the population of the $X^2\Pi_{1/2}$ spin–orbit state of $C_8H$ is less than 2%. In analysing the spectral information, the focus was on these cold spectra, where use can be made of a standard Hamiltonian restricted to the $^2\Pi_{3/2}$–$\widetilde{X}^2\Pi_{3/2}$ transition with neglect of the $^2\Pi_{1/2}$–$\widetilde{X}^2\Pi_{1/2}$ spin–orbit component.

Figure 2 shows contour fits performed for the $n = 4$ isotopologues. As stated above, the fitting results of the cold (∼7–9 K) spectra of $C_8H$, $C_8D$ and $^{13}C_8H$, as shown in the panels (a), (c) and (e) of Figure 2 are considered to be most reliable in view of the absence of contributions by the weaker spin–orbit component. The resulting parameters, as summarised in Table 1, are based on these cold spectra. A comprehensive fitting routine in which four variables – $B'$, $T_{00}$, Γ and $T_{rot}$ – are simultaneously fitted yields effective

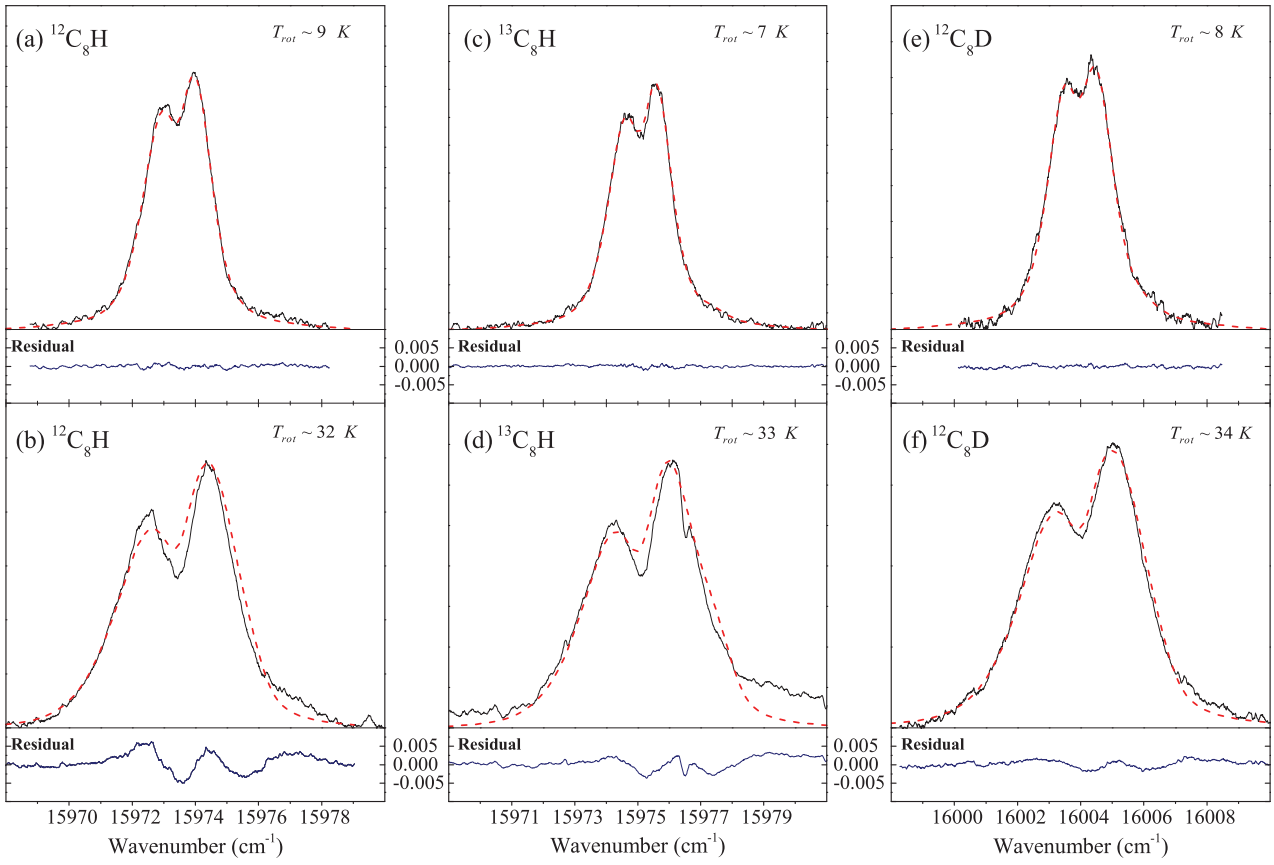


Figure 2. Low and high temperature spectra for the three band systems shown in Figure 1. The result of the contour plot fits is incorporated in red, using the constants listed in Table 1.

values for the Lorentzian line broadening parameters: $\Gamma = 0.79 \pm 0.10$ cm$^{-1}$ ($C_8H$), $\Gamma = 0.84 \pm 0.10$ cm$^{-1}$ ($C_8D$) and $\Gamma = 0.79 \pm 0.15$ cm$^{-1}$ ($^{13}C_8H$). The covariance matrix of these fits yields a low correlation between the variables; in particular, the result for the broadening parameter $\Gamma$ is well constrained and unaffected by correlations for these spectra of good S/N with a clearly resolved splitting between an R- and a P-branch. The spread in the $\Gamma$-values as obtained

Table 1. Effective constants derived (in cm$^{-1}$) from contour fit analyses of the $^2\Pi$–$\widetilde{X}^2\Pi$ electronic origin band spectra of $C_8H$, $C_{10}H$, $C_{12}H$ and their D- and $^{13}C$ fully substituted isotopologues. The digits in the parentheses represent the standard deviation of averaged values. The listed values are derived from the cold spectra largely representing the $^2\Pi_{3/2}$–$\widetilde{X}^2\Pi_{3/2}$ transition (see the text).

| | $\widetilde{X}^2\Pi$ ground state | $^2\Pi_{3/2}$ excited state | | | |
|---|---|---|---|---|---|
| | $B''$ | $B'$ | $T_{00}$ ($\Omega = 3/2$) | $T_{00} - T_{00(^{12}C_nH)}$ | $\Gamma$ |
| $C_8H$ | 0.019589011(3)[a] | 0.01938(2) | 15,973.5(2) | 0 | $0.79 \pm 0.10$ |
| $^{13}C_8H$ | 0.0181[b] | 0.01790(4) | 15,975.1(6) | ~2 | $0.79 \pm 0.15$ |
| $C_8D$ | 0.0189[b] | 0.01878(5) | 16,004.0(5) | ~30 | $0.84 \pm 0.10$ |
| $C_{10}H$ | 0.010053953(3)[a] | 0.0099[c] | 14,000.0(9) | 0 | $3.9 \pm 0.5$ |
| $^{13}C_{10}H$ | 0.0093[b] | 0.0092[c] | 14,000.2(6) | ~1 | $3.5 \pm 0.3$ |
| $C_{10}D$ | 0.0098[b] | 0.0097[c] | 14,019.4(5) | ~20 | $3.8 \pm 0.5$ |
| $C_{12}H$ | 0.005830162(3)[a] | 0.0058[c] | 12,646.4(5) | 0 | $4.7 \pm 0.7$ |
| $C_{12}D$ | 0.0055[b] | 0.0055[c] | 12,658.5(7) | ~12 | $4.8 \pm 0.5$ |

[a] From Ref. [12,14].
[b] DFT-calculated values for $B''_e$ and fixed in the contour fit.
[c] Estimated values (see the text).

from multiple recordings is small, thus leading to small uncertainty margins on the final result. The uncertainties given in Table 1 are related to cold spectra only, and are relatively small as temperature dependent interferences – i.e. contributions from the second spin–orbit component – can be neglected for temperatures as low as ~7–9 K.

The lifetime broadening parameter is consistent for all three isotopologues and amounts to $\Gamma = 0.8 \pm 0.1$ cm$^{-1}$ for the $n = 4$ species. This value correspond to a lifetime of ~7 ps for the upper $^2\Pi_{3/2}$ electronic state, in agreement with the value derived in Ref. [21].

As for the warmer spectra, with typical temperatures of 30 K and displayed in Figure 2(b), 2(d) and 2(f), the intensity contribution of the $^2\Pi_{1/2}$–$\widetilde{X}^2\Pi_{1/2}$ spin–orbit component must be accounted for, leading to a number of difficulties. These spectra show deviations from the simulations. In Refs [21,31], it was noticed that the rotationally resolved $\widetilde{A}^1A_2$–$\widetilde{X}^1A_1$ band system of *l*-$C_3H_2$ overlaps with the $C_8H$ band. However, careful inspection of the ~30 K spectra (displayed in Figure 1) shows that the *l*-$C_3H_2$ features are indeed observed, but at very low intensity and sharp. Therefore, they cannot explain the residuals in the higher temperature spectra. A possible alternative explanation for the residuals in the fits of warmer spectra is that the contribution of the upper spin–orbit transition becomes visible.

To model the warmer spectra, a simplification in the fitting routine is introduced by adopting the values for the molecular parameters $B'$ and $\Gamma$ as obtained from the cold spectra. In this case, the modelling involves a value for the excited-state spin–orbit constant $A'$ as an extra parameter in the fitting routine. As a further approximation, we performed fits for the warmer spectra with a fixed value of $A' = -20.5$ cm$^{-1}$, to comply with an estimate of $|A'' - A'| \leq 1.5$ cm$^{-1}$ as deduced in Ref. [20]. Figure 2(b), 2(d) and 2(f) shows the results of simulations for the warmer spectra, in which the rotational temperature $T_{rot}$ was optimised by fitting. These simulations validate the bound $|A'' - A'| \leq 1.5$ cm$^{-1}$ and the value of $T_{00}$ coinciding with that found for the colder spectra.

The spectra of the $n = 4$ species ($C_8H$, $C_8D$ and $^{13}C_8H$) provide an experimental correlation between the setting of the distance between the pinhole nozzle orifice and the optical cavity axis, and the internal temperature $T_{rot}$ of the molecular species detected downstream. With the assumption that the internal temperature relaxation of the molecular species studied here is not strongly molecule specific, this provides a handle on preparing the larger chain molecules of the $n = 5$ and $n = 6$ species at certain temperatures.

### 3.2. *$C_{10}H$, $C_{10}D$, $^{13}C_{10}H$ and $^{13}C_{10}D$*

Spectral recordings of the $^2\Pi$–$\widetilde{X}^2\Pi$ electronic origin band transitions of $C_{10}H$ and $C_{10}D$ are shown in Figure 3. The present S/N is better than that of the previously published spectra [20]. Also shown in Figure 3 is the $^2\Pi$–$\widetilde{X}^2\Pi$ band of $^{13}C_{10}H$, which is obtained from a $^{13}C$ enriched sample of precursor gas. The absorption peak near 14,020 cm$^{-1}$ has no equivalent in the $^{12}C$ spectra and is shown in the inset. It is blueshifted $\leq$1.0 cm$^{-1}$ with respect to $C_{10}D$, i.e., a

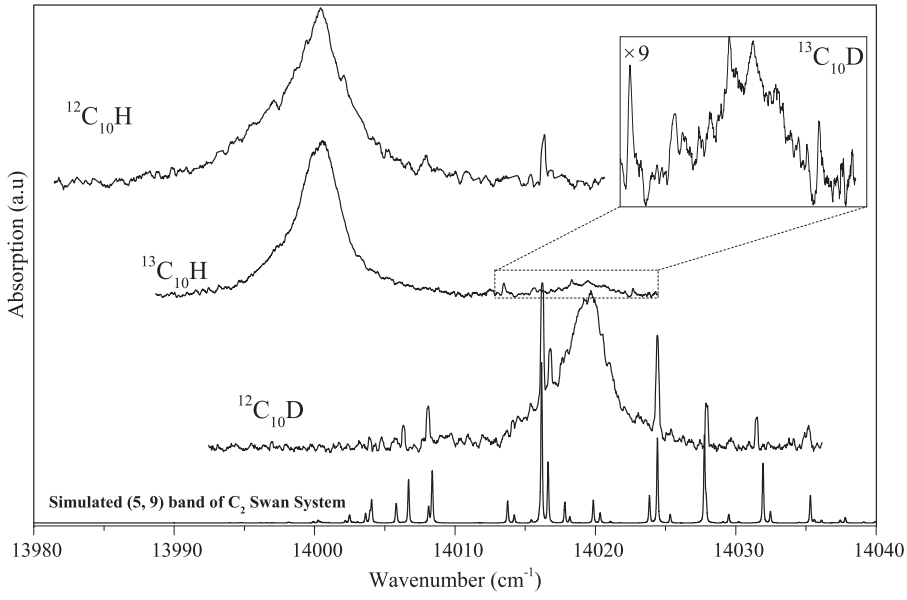


Figure 3. The $^2\Pi$–$\widetilde{X}^2\Pi$ electronic origin band transition of $C_{10}H$ (upper trace), $^{13}C_{10}H$ (middle trace) and $C_{10}D$ (lower trace) observed by cavity ring down spectroscopy in a pulsed pinhole jet plasma. The $C_{10}H$ and $C_{10}D$ spectra are partially blended with sharp absorption lines of $C_2$ as can be concluded from the simulated spectrum of the (5, 9) band of the $C_2$ Swan system.

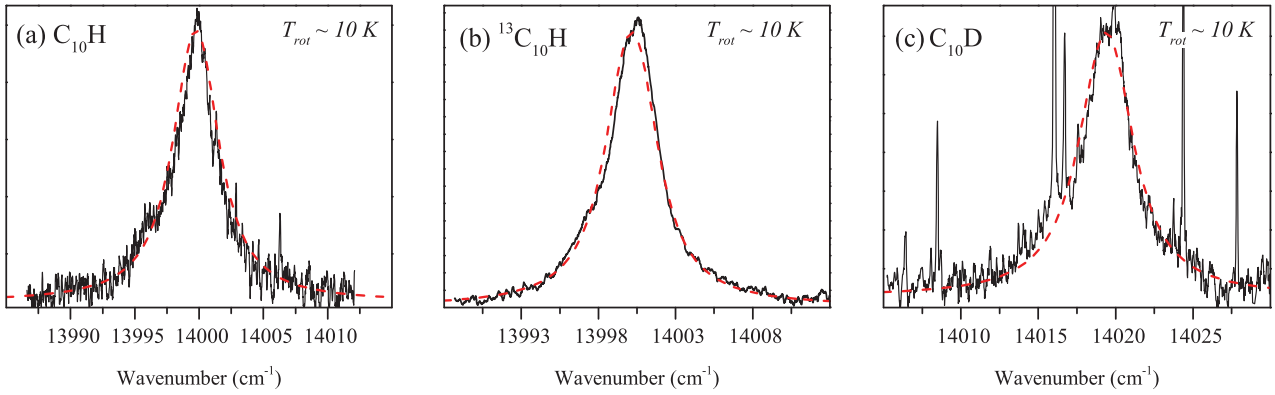


Figure 4. The cold spectra for the three band systems shown in Figure 3. The result of the contour plot fits for $T_{rot} = 10$ K is incorporated in red, using the constants listed in Table. 1.



value similar to the difference found for $C_{10}H$ and $^{13}C_{10}H$. Therefore, the explanation of this feature is fully consistent with an assignment to $^{13}C_{10}D$ and originates from the same pollution of precursor gas that was discussed above. Its resulting spectrum is not of sufficient quality to perform a contour fitting delivering significant results. The spectra of the $n = 5$ species are not expected to be rotationally resolved – the $2B$ ($\approx$0.03 cm$^{-1}$) separation is smaller than the achievable resolution – and moreover, the spectra are lifetime broadened as in the case of $C_8H$.

Several sharp features show up in the $C_{10}H$ and $C_{10}D$ spectra that are not found in a $^{13}C_2H_2$/Ar/He plasma and therefore must be due to $^{12}C$-containing species. Indeed, the simulated spectrum for the (5, 9) ro-vibronic band of the $^{12}C_2$ Swan system [26] – shown in Figure 3 – fully reproduces the observed transitions and is used for calibrating the spectra. For the contour fitting procedures to be carried out, these sharp features were not considered and effectively erased from the spectra.

The recorded $C_{10}H$, $C_{10}D$ and $^{13}C_{10}H$ spectra do not exhibit distinctive P- and R-branches and appear as a single unresolved bump structure. This makes the analysis of the spectra even more difficult than in the case of $C_8H$. A major difficulty encountered is that a simultaneous multi-parameter fitting analysis optimising the parameters $B'$, $T_{00}$, $\Gamma$ and $T_{rot}$ is no longer possible, not even for the coldest spectra.

The strategy chosen to analyse these spectra is to include as much as available a-priori knowledge and focus a fitting routine to extract information on the natural lifetime broadening of the upper electronic state. For the main $C_{10}H$ isotopologue, the ground-state rotational constant $B_0'' = 0.010054$ is taken from available microwave data [12]. For the $C_{10}D$ and $^{13}C_{10}H$ isotopologues, where no microwave data are available, the ground-state rotational constants are fixed to DFT-calculated values of $B_e'' = 0.009819$ and 0.009328 cm$^{-1}$, respectively. The ratio of $B''/B'$, derived from rotationally resolved spectra of $C_6H$ and $C_6D$ in Ref. [19], is consistent with the corresponding value found for $HC_6H^+$ and $DC_6D^+$ reported in Ref. [32]. Hence, the $B'$ values for $C_{10}H$, $C_{10}D$ and $^{13}C_{10}H$ are estimated from the ratio of $B''/B' = 1.007$ reported for their iso-electronic $HC_{10}H^+$ and $DC_{10}D^+$ species [32]. We assumed that the ratio of $B''/B'$ for $^{13}C_{10}H$ is the same as for $C_{10}H$. Accurate information for the spin–orbit constants $A''$ and $A'$ is not available for these isotopologues. However, as explained in the above section, this is not required for analysing the coldest spectra, where the contribution of the weaker $^2\Pi_{1/2}$–$\tilde{X}^2\Pi_{1/2}$ spin–orbit component can be safely neglected. In that case, the band origin $T_{00}$ represents the splitting between the $\Omega = 3/2$ components in ground and excited electronic states. Based on this list of assumptions, the coldest accessible spectra are analysed by contour fitting, aiming to derive the values of the Lorentzian line widths $\Gamma$ and the band origins $T_{00}$ for the molecules in the $n = 5$ species.

Figure 4 shows the observed and simulated cold spectra for $C_{10}H$, $C_{10}D$ and $^{13}C_{10}H$ using the DFT-calculated and estimated values as listed in Table 1. The best contour fits are realised for Lorentzian line widths of $\Gamma = 3.9 \pm 0.5$ cm$^{-1}$ for $C_{10}H$, $\Gamma = 3.8 \pm 0.5$ cm$^{-1}$ for $C_{10}D$ and $\Gamma = 3.5 \pm 0.3$ cm$^{-1}$ for $^{13}C_{10}H$. These fits were performed for a temperature setting of 10 K, as was established from the nozzle–optical axis setting in the previous $C_8H$ experiment. Again, it should be noted that the analysis is based on the calculated values for $B''$ and $B'$, and the neglect of population of the $^2\Pi_{1/2}$ component. It was verified that the simulated spectra are not sensitive for the exact temperature setting and reproduce the experimental features for settings in the window $T_{rot} = 5$–15 K. The resulting $\Gamma = 4.0$ cm$^{-1}$ corresponds to a lifetime of about $\sim$1.3 ps for the upper $^2\Pi_{3/2}$ electronic state, and is shorter than found for $C_8H$. Good agreement is found between the observed spectra and the fitted contours.

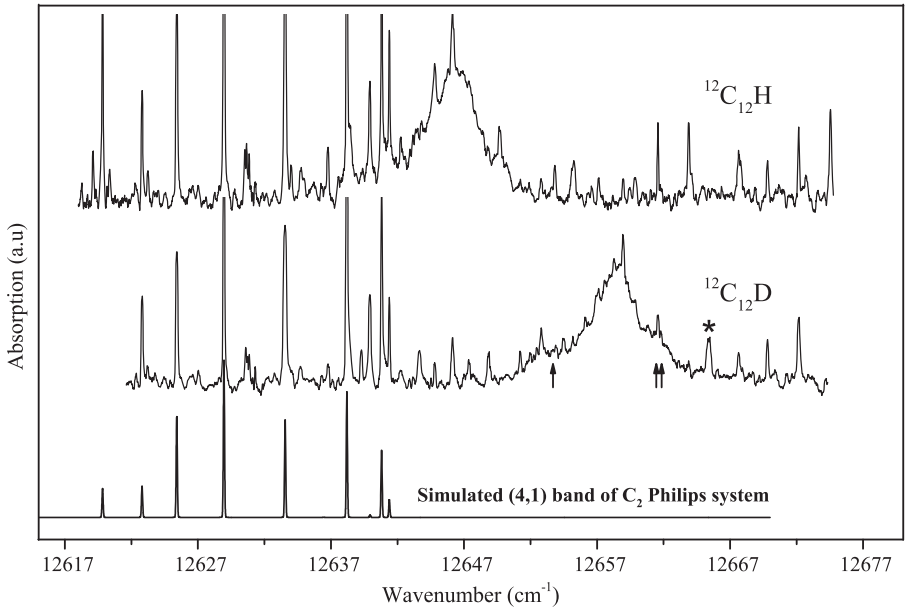


Figure 5. The $^2\Pi$–$\widetilde{X}^2\Pi$ electronic origin band transition of $C_{12}H$ (upper trace) and $C_{12}D$ (lower trace) observed by CRDS in a pulsed pinhole jet plasma. The origin of the side-bands to the main peak in the $C_{12}D$ spectrum, marked by arrows, is unknown (see text). Polluting transitions on the left are due to (4, 1) band transitions of the $C_2$ Philips system as shown in the simulated spectrum (bottom trace), while the weaker sharp lines on the right have not been identified. The line marked with an asterisk (⋆) is most likely due to CD.

### 3.3. $C_{12}H$, $C_{12}D$

Spectral recordings of the gas-phase $^2\Pi$–$\widetilde{X}^2\Pi$ electronic origin band transitions of $C_{12}H$ and $C_{12}D$ are shown in Figure 5. The spectra exhibit a better S/N than available from the previous studies [22,23]. Also for these carbon-chain molecules in the $n = 6$ species, for which adjacent rotational lines are expected to be split by only 0.01 $cm^{-1}$, rotational structures cannot be resolved due to the combination of limited laser bandwidth and the Doppler broadening in the pinhole jet expansion, while also lifetime broadening is expected. For these reasons, the spectra appear as unstructured single bump features.

The $C_{12}H$ to $C_{12}D$ isotopic shift amounts to ∼12 $cm^{-1}$, which is less than the ∼20 and ∼30 $cm^{-1}$ shifts found for $C_{10}H$ and $C_8H$, respectively. We tried to record a spectrum for the $^{13}C_{12}H$ species applying similar settings as used for $^{13}C_8H/D$ and $^{13}C_{10}H/D$, but did not succeed. Again, spectral overlap exists with transitions that originate from small radicals. In this specific case, the features observed in the range 12,617–12,640 $cm^{-1}$ arise from the (4, 1) band of the $C_2$ Philips system as shown in the lower trace of Figure 5. The features in the range 12,640–12,670 $cm^{-1}$ have not been fully identified.

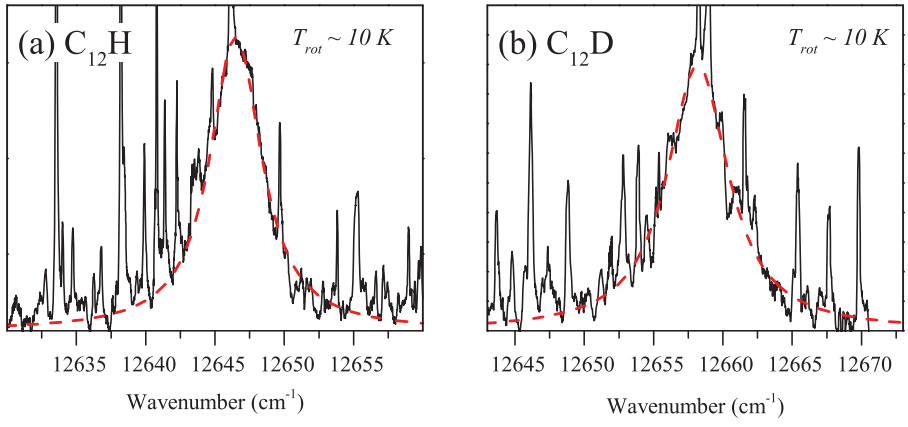


Figure 6. The cold spectra for the two bands shown in Figure 5. The result of the contour plot fits for $T_{rot} = 10$ K is incorporated in red, using the constants listed in Table. 1.

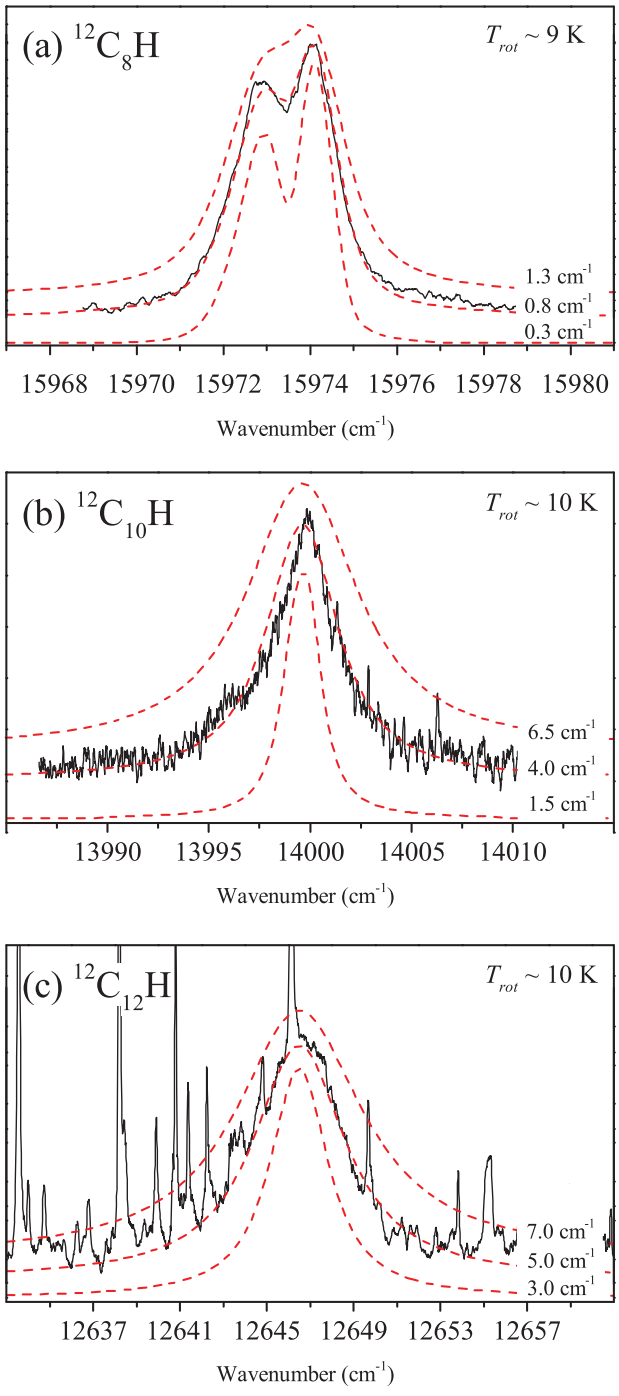


Figure 7. A systematic variation of the lifetime broadening parameter for $C_8H$ (a), $C_{10}H$ (b) and $C_{12}H$ (c) overlapped with the recorded spectra presented here.

Figure 6 shows the observed cold spectra for $C_{12}H$ and $C_{12}D$. As in the previous sections, contour fitting has been applied for several cold spectra using a standard $^2\Pi_{3/2}$–$^2\Pi_{3/2}$ Hamiltonian. The recorded $C_{12}H$ and $C_{12}D$ spectra are analysed following similar procedures as laid out for $C_{10}H$ and $C_{10}D$.

The rotational constant $B''$ of $C_{12}H$ in its $\tilde{X}^2\Pi$ ground electronic state is known from microwave spectroscopy [12], while for $C_{12}D$ a value of $B''_e = 0.005558$ cm$^{-1}$ has been determined from our DFT calculations. Different from the case of $C_{10}H$ discussed above, the $B''/B'$ for the isoelectronic $HC_{12}H^+$ is not reported. However, based on the discussion in Ref. [32] that the $B''/B'$ ratio decreases with increasing chain length, a $B''/B'$ value of about 1.002 can be extrapolated for $HC_{12}H^+$ from the constants derived for shorter $HC_{2n}H^+$ species [32]. Here, this ratio is used to estimate the excited-state constants $B'$ for $C_{12}H$ and $C_{12}D$.

Contour fits are performed to the experimental spectra by fixing the $B''$ and $B'$ rotational constants to DFT-calculated and estimated values, while $T_{00}$ as well as Lorentzian line widths $\Gamma$ are varied to reproduce the spectra. Again, it is assumed that the effect of spin–orbit interaction can be neglected for the cold spectra with population in the inverted $\tilde{X}^2\Pi_{3/2}$ ground state only. Optimised contours for $C_{12}H$ and $C_{12}D$ are obtained for the values listed in Table 1. Lorentzian line widths of $\Gamma = 4.7 \pm 0.7$ cm$^{-1}$ for $C_{12}H$ and $\Gamma = 4.8 \pm 0.5$ cm$^{-1}$ for $C_{12}D$ are determined and found to be uncorrelated with other fit parameters, yielding an upper $^2\Pi_{3/2}$ state lifetime of ~1.1 ps for $n = 6$ species.

In the warmer spectra of $C_{12}D$, at internal temperatures of $T_{rot} \sim 30$ K estimated from the nozzle-to-optical axis setting, two shoulders appear as side-band features – indicated with single and double arrows in Figure 5. These features do not appear in the spectra of $C_{12}H$ and are also not visible in the spectra recorded at lower temperatures of $T_{rot} < 10$ K, so they do not affect the contour fitting analysis and the lifetime determinations. As there seems to be a temperature dependency involved, explanations of these features may range from a hot band or a higher population of the upper spin–orbit component. A possible alternative explanation for these shoulders is that they are related to other species simultaneously generated in the plasma. At this stage, this observation cannot be explained.

## 4. Discussion and conclusions

The results for $^{12}C_{8/10}H(D)$ and $^{13}C_{8/10}H(D)$ presented here demonstrate that the isotopic shifts of the $^{13}C$-substituted carbon chains $C_{2n}H$ exhibit a similar trend as for the H/D shifts of other hydrocarbon chains with the shift decreasing with increasing chain length [33,34]. In addition, the $^{13}C$ isotopic shifts are about one order smaller than those found for deuterated species. It is difficult to accurately predict the isotopic shifts, since the centre shift of an electronic origin transition band originates from the change of the vibrational zero-point energy in both ground and excited electronic states upon isotope (D or $^{13}C$) substitution [33,34].

It may seem counterintuitive to extract a value for the lifetime broadening from a rotationally unresolved contour, where the exact value for the excited-state rotational

constant is lacking and the rotational temperature is not accurately known. However, for all the individual analyses, it was verified that the extracted values of the lifetime broadening were not sensitively dependent on the estimated or DFT-calculated values for the rotational constants. In Figure 7, additional material is shown to graphically illustrate the determination of the line broadening parameters Γ in each of the contour-fitted spectra of $C_8H$, $C_{10}H$ and $C_{12}H$. The contour fits are recalculated for varying Γ parameters in a range around the optimum values as listed in Table 1. This procedure is in fact repeated (not shown) for spectra recorded at different temperature settings, confirming reliable and consistent values for the line broadening.

The interesting outcome of the present experimental study on the spectra of long $^{12/13}C_{2n}H/D$ carbon-chain molecules, therefore is that even for the unresolved spectra an effective lifetime broadening can be deduced, by fixing the spectroscopy in the fit making quite straight forward assumptions. The Γ values are derived for 'ideal spectra', i.e., low temperature spectra, where the influence of interfering patterns can be largely neglected. The resulting lifetime broadening values for $C_{10}H$ and $C_{12}H$ are larger than found for $C_8H$ and the latter value is again larger than concluded from fully rotationally resolved spectra of $C_6H$, where actually no proof for lifetime broadening was found. These observations are independent of isotopic composition, and can in principle be ascribed to either pre-dissociation or internal non-radiative decay. In view of the low excitation energies of the excited states and the dissociation products of such linear carbon chains carrying higher internal energies, the short lifetimes of the carbon-chain species investigated must be due to intramolecular energy conversion/redistribution processes, likely governed by resonant or non-resonant perturbations, possibly even complex state mixing. In the energy region of the excited $^2\Pi$ state, the total vibronic-state density of such long chains containing more than nine atoms is expected to be sufficiently large to explain our observations.


## Acknowledgements

This work has been performed as part of ongoing research within the Dutch Astrochemistry Network.

## Funding

This work was financially supported by the Netherlands Foundation for Fundamental Research of Matter (FOM) [grant program 125]; the Netherlands Research School for Astronomy (NOVA); the 'Stichting Physica'.


## References


[1] P. Thaddeus, C.A. Gottlieb, A. Hjalmarson, L.E. Johansson, W.M. Irvine, P. Friberg, and R.A. Linke, Astrophys. J. **294**, L49 (1985).

[2] M. Guélin, S. Green, and P. Thaddeus, Astrophys. J. **224**, L27 (1978).

[3] J. Cernicharo, C. Kahane, J. Gomez-Gonzalez, and M. Guélin, Astron. Astrophys. **164** (1), L1–L4 (1986).

[4] H. Suzuki, M. Ohishi, N. Kaifu, S.I. Ishikawa, and T. Kasuga, Publ. Astron. Soc. Jpn. **38** (6), 911–917 (1986).

[5] M. Guélin, J. Cernicharo, M.J. Travers, M.C. McCarthy, C.A. Gottlieb, P. Thaddeus, M. Ohishi, S. Saito, and S. Yamamoto, Astron. Astrophys. **317** (1), L1–L4 (1997).

[6] J. Cernicharo and M. Guélin, Astron. Astrophys. **309** (2), L27–L30 (1996).

[7] S. Brünken, H. Gupta, C.A. Gottlieb, M.C. McCarthy, and P. Thaddeus, Astrophys. J. Lett. **664** (1), L43–L46 (2007).

[8] M.B. Bell, P.A. Feldman, J.K.G. Watson, M.C. McCarthy, M.J. Travers, C.A. Gottlieb, and P. Thaddeus, Astrophys. J. **518** (2), 740–747 (1999).

[9] J. Cernicharo, M. Guélin, M. Agúndez, K. Kawaguchi, M.C. McCarthy, and P. Thaddeus, Astron. Astrophys. **467** (2), L37–L40 (2007).

[10] M.C. McCarthy, C.A. Gottlieb, H. Gupta, and P. Thaddeus, Astrophys. J. Lett. **652** (2), L141–L144 (2006).

[11] K. Kawaguchi, R. Fujimori, S. Aimi, S. Takano, E. Okabayashi, H. Gupta, S. Brünken, C.A. Gottlieb, M.C. McCarthy, and P. Thaddeus, Publ. Astron. Soc. Jpn. **59** (5), L47–L50 (2007).

[12] C.A. Gottlieb, M.C. McCarthy, M.J. Travers, J. Grabow, and P. Thaddeus, J. Chem. Phys. **109** (13), 5433–5438 (1998).

[13] M.C. McCarthy, W. Chen, A.J. Apponi, C.A. Gottlieb, and P. Thaddeus, Astrophys. J. **520** (1), 158–161 (1999).

[14] M.C. McCarthy, M.J. Travers, A. Kovacs, C.A. Gottlieb, and P. Thaddeus, Astrophys. J. Suppl. Ser. **113**, 105 (1997).

[15] P. Freivogel, J. Fulara, M. Jakobi, D. Forney, and J.P. Maier, J. Chem. Phys. **103** (1), 54–59 (1995).

[16] C.A. Rice and J.P. Maier, J. Chem. Phys. A. **117** (27), 5559–5566 (2013).

[17] A. Walsh, D. Zhao, W. Ubachs, and H. Linnartz, J. Phys. Chem. A **117** (39), 9363–9369 (2013).

[18] H. Linnartz, T. Motylewski, O. Vaizert, J.P. Maier, A.J. Apponi, M.C. McCarthy, C.A. Gottlieb, and P. Thaddeus, J. Mol. Spectrosc. **197** (1), 1–11 (1999).

[19] D. Zhao, M.A. Haddad, H. Linnartz, and W. Ubachs, J. Chem. Phys. **135** (4), 044307 (2011).

[20] H. Linnartz, T. Motylewski, and J.P. Maier, J. Chem. Phys. **109** (10), 3819–3823 (1998).

[21] P. Birza, D. Khoroshev, A. Chirokolava, T. Motylewski, and J.P. Maier, Chem. Phys. Lett. **382** (3–4), 245–248 (2003).

[22] T. Motylewski, Ph. D. thesis, University of Basel, 2001.

[23] T. Motylewski, H. Linnartz, O. Vaizert, J.P. Maier, G. Galazutdinov, F.A. Musaev, J. Krełowski, G.A.H. Walker, and D.A. Bohlender, Astrophys. J. **531** (1), 312–320 (2000).

[24] D. Zhao, N. Wehres, H. Linnartz, and W. Ubachs, Chem. Phys. Lett. **501** (4), 232–237 (2011).

[25] M.A. Haddad, D. Zhao, H. Linnartz, and W. Ubachs, Chin. J. Chem. Phys. **25** (2), 129–134 (2012).

[26] S.H. Yeung, M.C. Chan, N. Wang, and A.S.C. Cheung, Chem. Phys. Lett. **557**, 31 (2013).

[27] M. Chan, Chem. Phys. Lett. **390** (4–6), 340–346 (2004).

[28] M.A. Haddad, D. Zhao, H. Linnartz, and W. Ubachs, J. Mol. Spectrosc. **297**, 41 (2014).

[29] C. M. Western, PGOPHER, a program for simulating rotational structure, University of Bristol. <http://pgopher.chm.bris.ac.uk>.

[30] M.J. Frisch, G.W. Trucks, H.B. Schlegel, G.E. Scuseria, M.A. Robb, J.R. Cheeseman, J.A. Montgomery, Jr., T. Vreven, K.N. Kudin, J.C. Burant, J.M. Millam, S.S. Iyengar, J. Tomasi, V. Barone, B. Mennucci, M. Cossi, G. Scalmani, N. Rega, G.A. Petersson, H. Nakatsuji, M. Hada, M. Ehara, K. Toyota, R. Fukuda, J. Hasegawa, M. Ishida, T. Nakajima,

Y. Honda, O. Kitao, H. Nakai, M. Klene, X. Li, J.E. Knox, H.P. Hratchian, J.B. Cross, C. Adamo, J. Jaramillo, R. Gomperts, R.E. Stratmann, O. Yazyev, A.J. Austin, R. Cammi, C. Pomelli, J.W. Ochterski, P.Y. Ayala, K. Morokuma, G.A. Voth, P. Salvador, J.J. Dannenberg, V.G. Zakrzewski, S. Dapprich, A.D. Daniels, M.C. Strain, O. Farkas, D.K. Malick, A.D. Rabuck, K. Raghavachari, J.B. Foresman, J.V. Ortiz, Q. Cui, A.G. Baboul, S. Clifford, J. Cioslowski, B.B. Stefanov, G. Liu, A. Liashenko, P. Piskorz, I. Komaromi, R.L. Martin, D.J. Fox, T. Keith, M.A. Al-Laham, C.Y. Peng, A. Nanayakkara, M. Challacombe, P.M.W. Gill, B. Johnson, W. Chen, M.W. Wong, C. Gonzalez, and J.A. Pople, GAUSSIAN 03, Revision C.02 (Gaussian Inc., Pittsburgh, PA, 2003).

[31] P. Birza, A. Chirokolava, M. Araki, P. Kolek, and J.P. Maier, J. Mol. Spectrosc. **229** (2), 276–282 (2005).

[32] P. Cias, O. Vaizert, A. Denisov, J. Mes, H. Linnartz, and J.P. Maier, J. Phys. Chem. A **106** (42), 9890–9892 (2002).

[33] D. Zhao, H. Linnartz, and W. Ubachs, J. Chem. Phys. **136** (5), 054307 (2012).

[34] C.D. Ball, M.C. McCarthy, and P. Thaddeus, J. Chem. Phys. **112** (23), 10149–10155 (2000).